CNN-based Quantification of Blood Vessels Lumen in 3D Images*

Andrzej Materka[1][0000−0003−0864−1518], Jakub Jurek[1][0000−0003−4008−5267],
Marek Kocinski[2,3,1][0000−0001−7088−4823], and Artur
Klepaczko[1][0000−0003−4045−5870]

[1] Lodz University of Technology, Institute of Electronics, Lodz 90-924, Poland
`materka@p.lodz.pl`, http://www.eletel.p.lodz.pl
[2] University of Bergen, Bergen, Hordaland, Norway
[3] Mohn Medical Imaging and Visualization Centre, Bergen, Hordaland, Norway

Abstract. The aim of this work is to develop a method for automated, fast and accurate geometric modeling of blood vessels from 3D images, robust to image limited resolution, noise and artefacts. Within the centerline-radius paradigm, convolutional neural networks (CNNs) are used to approximate the mapping from the image cross-sections to vessel lumen parameters. A six-parameter image formation model is utilized to derive conditions for this mapping to exist, and to generate images for the CNN training, validation and testing. The trained networks are applied to real-life time-of-flight (TOF) magnetic resonance images (MRI) of a blood-flow phantom. Excellent agreement is observed between the predictions made by the CNN and those obtained via model fitting as the reference method. The latter is a few orders of magnitude slower than the CNN and suffers from local minima problem. The CNN is also trained and tested on publicly available contrast-enhanced (CE) computed tomography angiography (CTA) clinical datasets. It accurately predicts the coronary-tree lumen parameters in seconds, compared to hours needed by human experts. The method can be an aid to vascular diagnosis and automated annotation of images.

Keywords: Medical image analysis · CNN · Parameter estimation · Blood-vessels lumen modeling · Centerline-radius paradigm · Uncertainty.

1 Introduction

Cardiovascular disease produces immense health and economic burdens globally [1]. The main types of this disease originate from blocked blood supply to organs and tissues. The related clinical practices rely on angiography and venography in multiple imaging modalities to acquire information about human vascularity. Reliable quantification and visualization of vascular structures is important for diagnosis assistance, treatment, surgery planning/execution, pathology

---

quantification, and evaluation of clinical outcomes in different fields, including laryngology, neurosurgery and ophthalmology [2], [3]. Three-dimensional imaging is the main technique used to acquire quantitative information about the vasculature. Example modalities include MR angiography (MRA) which can be flow-dependent (TOF or phase contrast angiography) or flow-independent. An invasive alternative is computed tomography angiography (CTA). They can both be contrast-enhanced (CE) or nonenhanced. Various diseases require the usage of dedicated imaging techniques and image analysis algorithms. The most often considered abnormalities are stenosis, aneurysms and calcifications [2].

The human vasculature exhibits a complex tree-like structure of highly-curved, different-diameter branches. They are closely surrounded by other arteries, veins and tissues. The images feature limited spatial resolution and substantial noise. These factors make the tasks of vessel quantification in 3D images especially challenging for radiologists. Manual vessel labeling is tedious, time-consuming and error-prone [4]. There is a strong need to develop automated techniques for accurate, fast and objective vascularity evaluation [3] – to relieve radiologists of the burden of adding annotations to 3D images, crucial to effectively train data-driven solutions for healthcare. The main difficulties in achieving this task are in limited spatial resolution, intensity variations in regions surrounding the vessels, and imaging artefacts. These nonidealities increase uncertainty of lumen geometry measurements. The aim of this study is to develop a robust algorithm for fast, quantitative, subpixel-accuracy geometric characterization of blood vessels' lumen, given their 3D image.

There are two main approaches to vascular structures segmentation and quantification in 3D images [5], [6]:

- direct volumetric lumen segmentation,
- 2D cross-sectional characterization along approximate centerline.

We focus on the second method and use a CNN to estimate of the lumen parameters from image cross-sections. The first approach is usually performed with the use of time-consuming calculations [7] or much faster convolutional neural networks [8]. Still, the segmentation produces images which are a coarse, voxelized representation of the vessel, with a need for postprocessing aimed at smooth approximation of its surface, e.g. for blood-flow simulation.

In our approach, the lumen cross-sections are computed as 2D images on planes perpendicular to the vessel centerline approximated by a smooth curve in 3D space [9] beforehand. This is less troublesome than volumetric segmentation of the lumen; various algorithms are available [10], [11]. Normal vectors to the centerline define the cross-section planes. The 2D images on such planes are obtained through the 3D discrete image interpolation and resampling. Alternatively, a lumen cross-section model is fitted to the image data for centerline-based vessel quantification, e.g. with the use of the least-squares (LS) algorithm [9]. This involves long-lasting iterative minimization of a nonlinear error function and is likely to get stuck in its local minima. We will use it as a reference method.

In Section 2, we describe the proposed method of lumen cross-section quantification. Section 3 characterizes the 3D image datasets to which the method is

applied to investigate its properties. The results are presented in Section 4, their discussion and conclusions form the content of Section 5.

2   Methods and materials

To study the problem, it is first assumed that the blood-vessel cross-section forms a circle of radius varying along the centerline. The hypothetical noiseless analog image $F(x, y)$ of the lumen cross-section, at any point (ξ, η, ζ) in the 3D space is a convolution of the imaging system effective impulse response $h(x, y)$ with the function $f(x, y)$ representing the lumen and its background

$$F(x, y) = \int_{-\infty}^{\infty} \int_{-\infty}^{\infty} f(u, v) h(x - u, y - v) dv du \tag{1}$$

where (x, y) are image coordinates on the cross-section plane, $(x, y) = (0, 0)$ at (ξ, η, ζ). The function $f(x, y)$ is constant within the lumen region, surrounded by the background of different, also constant, intensity. The function $h(x, y)$, assumed isotropic Gaussian, combines the effects of the 3D image scanner point-spread function (PSF) and interpolation which precedes 3D image resampling. These assumptions are relevant to many practical situations [12]. Other image formation model options (non-circular shape, non-constant lumen/background intensities) will be accounted for later on in this paper.

The equidistant sampling points on a Cartesian grid are $(x_i^s, y_j^s) = (i\Delta_s, j\Delta_s)$, $i, j \in \{-N, \ldots, 0, \ldots, N\}$, Δ_s denotes the sampling interval, and the cross-section image size is $(2N + 1) \times (2N + 1)$. The image intensity at (i, j) is the sampled convolution (1) multiplied by lumen intensity step b and added to the background intensity a. The circle center is shifted by (d_x, d_y) from the centerline. There are $P = 6$ image model parameters $\boldsymbol{\theta} = (\theta_0, \theta_1, \theta_2, \theta_3, \theta_4, \theta_5) = (a, b, R, w, d_x, d_y)$

$$I(i, j; \boldsymbol{\theta}) = a + bF(i\Delta_s - d_x, j\Delta_s - d_y, R, w). \tag{2}$$

where R and w denote, respectively, the lumen radius and the Gaussian "sigma".

The proposed method uses the CNN as a nonlinear regressor. The input to such network is the vessel cross-section image. Values of the model parameters are predicted at the CNN outputs. The network can be trained to estimate a single parameter or a number of them in $[1, \ldots, P]$. A cascade of three convolutional layers and three dense layers was used in the experiments, Fig. 1, where $N = 7$. The numbers of channels $N1, \ldots, N6$ in the layers depended on the estimated parameter(s) and image noise level.

In the transfer-learning training phase, the assumed parameter values are substituted to (2) to calculate image model intensity on a predefined sampling grid. This results in a noiseless image. Gaussian noise $\boldsymbol{\epsilon}$ is added to it, to take account of the uncertainty of measurement/reconstruction. Then, the neural network is trained to estimate the model parameters for images at its input. The CNN-predicted parameter values differ from those used to compute the input images. Sum-of-squares of these differences is the goal function minimized in the training process.
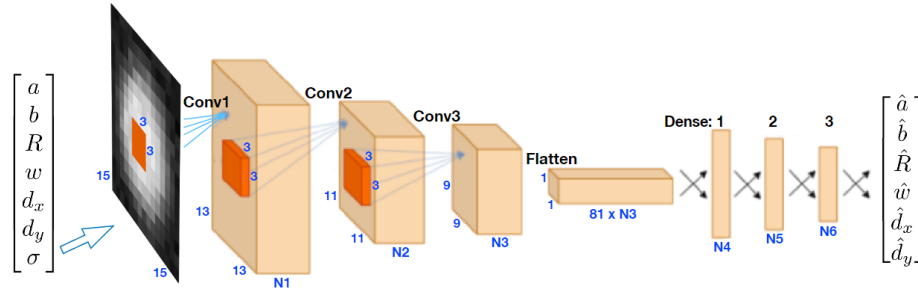
Fig. 1: CNN architecture applied to parameter estimation of blood-vessel lumen visualized in its 15×15-pixel 2D cross-section. The convolutional and dense layers feature ReLU activation functions, the output is linear.

In the recall phase, the neural network is driven by an image of unknown parameters and estimates their values. Ideally, the implicit input-output function $\hat{\boldsymbol{\theta}} = \boldsymbol{g}(\boldsymbol{\theta})$ of the pipeline in Fig. 1 should be an identity. Including bias and random noise components makes it more realistic:

$$\hat{\theta}_p \cong \theta_p + \beta_p + \nu_p, \qquad p \in \{0, \dots, P-1\} \tag{3}$$

where $\boldsymbol{\theta}$ is the vector of true values of the model parameters. The added terms of bias $\boldsymbol{\beta}$ and noise $\boldsymbol{\nu}$ depend on $\boldsymbol{\theta}$, image noise $\boldsymbol{\epsilon}$, sampling interval Δ_s, image artefacts, model adequacy, and numerical errors. Due to the complexity of the model equations (1) and (2), explicit derivation of the inverse mapping seems to be an impossible task. This justifies the use of a CNN to learn this mapping from example images of known parameters. The CNN ability to reconstruct it is limited by the finite number of layers and count of trainable weights, being another source of the estimator uncertainty. Sensitivity analysis [13] and Monte Carlo simulations were applied to (2) to find parameter subspaces and image sampling patterns where the inverse mapping exists, and to evaluate estimator bias and variance. Importantly, this estimator has much better precision (quantified with the RMS error) than implied by Cramér-Rao lower bound of unbiased predictors. Discussion of these findings extends beyond the scope of this paper.

The performance of the proposed lumen quantification method is assessed through its application to images of real blood vessels and their physical models. The MR-QA123 flow phantom, driven by computer-controlled pump was used to force a steady flow (2.5 ml/s) of blood-mimicking liquid through the lumen of the phantom branches [14]. The U-shaped 8 mm inner diameter pipe of the phantom is used in this work. The phantom was placed in a GE Signa HDxt 1.5T system. Fig. 2a shows a maximum-intensity-projection (MIP) of the pipe TOF image. Its voxel dimensions are $(0.82 \times 0.82 \times 1.01)$ mm³. Image intensity is normalized to $[0, 1]$. To assess the CNN performance on clinical images, 17 annotated datasets available as part of Rotterdam Coronary Artery Algorithms Evaluation Framework [4] are used. The volumes intensity is clipped to $[-300, 800]$ HU and normalized to $[0, 1]$.
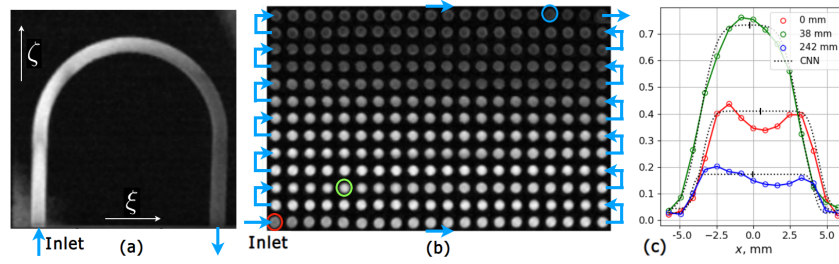
Fig. 2: Scanner-acquired TOF MRI for U-shaped pipe in flow phantom; a) MIP on the $0\xi\zeta$ plane, b) mosaic of lumen cross-sections (not to scale, arrows indicate fluid flow direction), c) 1D intensity profiles at $y = 0$ of sections taken at $d_c = 0, 38$, and 242 mm from inlet (marked respectively by red, green and blue circles in (b) and Fig. 3 upper row), black dotted lines: profiles reconstructed by model (2) supplied with CNN-predicted parameters.

3   Results

Prior to CNN training, the noise of the phantom images was found to be Gaussian with $PSNR \cong 30$dB. A pseudo-random noise of the corresponding standard deviation was added to each synthesized 2D cross-section in the training, validation, and testing sets. The 15×15-pixel images were computed using (2). For $\Delta_s = 0.82$ mm, the model parameters spanned randomly the ranges: $0 \leq a \leq 0.3$; $0.1 \leq b \leq 1.1$; $1.0 \leq R/\Delta_s \leq 6.0$; $0.3 \leq w/\Delta_s \leq 1.5$; $-1.2 \leq d_x/\Delta_s \leq 1.2$; $-1.2 \leq d_x/\Delta_s \leq 1.2$, with uniform probability distribution. The image counts in the three sets were 60 000, 20 000 and 20 000, respectively.

Five neural networks were trained: four single-ouput, each for a, b, R, w individual parameters, and one with two outputs for (d_x, d_y). The CNNs were implemented in Keras environment on a desktop computer with 16 GB RAM, Intel™ i5-8300H CPU @2300 MHz under MS Windows 11 OS. Computations were accelerated by NVIDIA GeForce GTX 1050 card with 4 GB GPU memory. Typical learning process (Adam weight optimization up to the time of validation error increase) took less than one hour, for (32,32,32,32,16,8) channels in the CNN layers. Computing the network output required 25 μs on average. The LS method was implemented with *least_squares*() function of the Scipy library, taking a minute to fit the model to a section of the pipe image.

Excellent agreement between the CNN and LS predictions for all six parameters is achieved, Fig. 3. The effect of stripe artefacts is clearly visible for $d_c \in [0, 100]$ mm, Fig. 3 left column (periodically varying lumen intensity b along the centerline). The two estimators differ more in the second half of the pipe, where the TOF SNR is low (due to flow direction reversal w.r.t. the 0ζ axis, Fig. 2a). This concerns especially $\hat{d}_x$ and $\hat{d}_y$ parameters; however, the disparity stays in the subvoxel range.

For each selected point of a coronary artery segment in CE-CTA images, the annotations include three lumen contours marked by respective observers on a
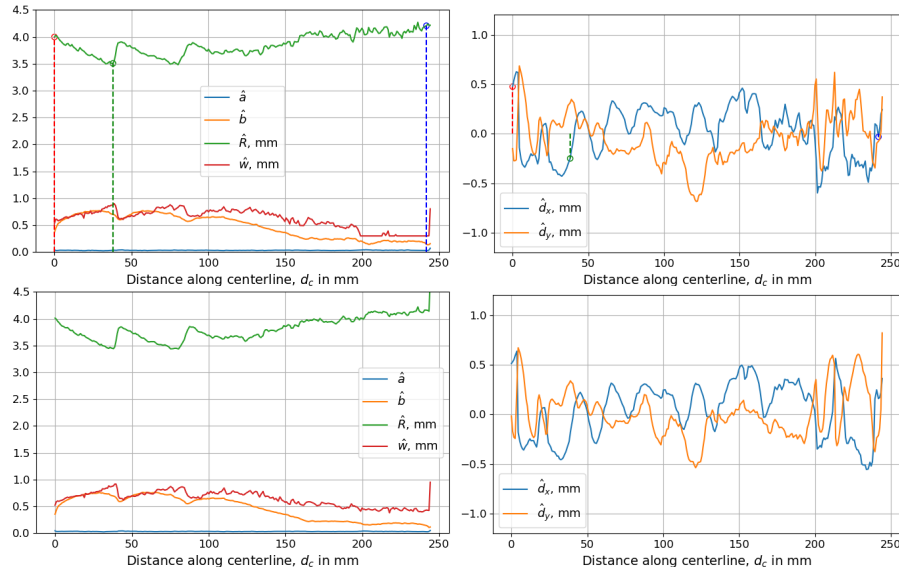
Fig. 3: Plots of estimated lumen parameters for MR TOF image of U-shaped pipe in the flow phantom, flow rate 2.5ml/s. Left: $\hat{a}, \hat{b}, \hat{R}, \hat{w}$; right: $\hat{d}_x, \hat{d}_y$. Top: CNN, red, green and blue marks correspond to sections encircled in Fig. 2b; bottom: LS model fitting. CNN trained on synthetic images at $PSNR = 30$dB.

common plane, orthogonal to an agreed centerline, Fig. 4. The contours allow computation of the section equivalent radius $\rho_k^{(o)} = \sqrt{A_k^{(o)}/\pi}$, where $A_k^{(o)}$ denote the area inside the contour, $o = 1, 2, 3$ and k is the section index. Their centers of mass provide coordinates of centerline points according to observers, Fig. 4 red dots. The image intensity is not constant over the background region, Fig. 4. This causes convergence difficulties of LS model fitting, leading to errors and excessive time of computation. The CNN is trained on real, nonideal images to make it insensitive to spurious objects in the background.

Example results of training and testing a CNN for equivalent radius estimation are shown in Fig. 5 for contours marked by Observer #1 on datasets #0, #1, #3, #4, #5, #6 (558 sections). Testing was done on 51 sections of three segments excluded from the training set. The mean absolute error (MAE) over the training and test sets was 0.13 mm and 0.11 mm, respectively. Similarly, MAE was less than 0.09 mm over the training set for each of d_x and d_y parameters, and it did not exceed 0.1 mm for the test set. Thus, subpixel accuracy is achieved for the CE-CTA as well ($\Delta_s = 0.45$ mm in this case).

4   Summary and conclusion

The CNN-based parameter predictions are in excellent agreement with the well-established LS method, for images whose appearance is close to the lumen model

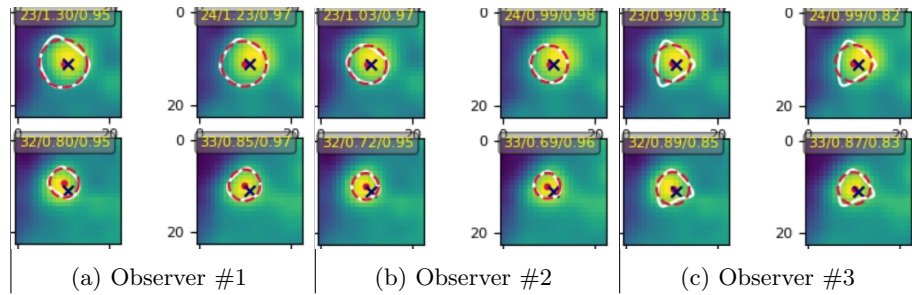(a) Observer #1   (b) Observer #2   (c) Observer #3

Fig. 4: Example lumen contours marked by three observers on sections $k = 23, 24, 32, 33$ of artery segment #8 in CE-CTA dataset #5. Blue cross: agreed reference centerline, white line: manually marked contour, red dot: computed contour centroid, red dashed line: equivalent circle.

of clear object and background (like TOF MR of the flow phantom, Fig. 2bc). Although the time of CNN training can be substantial, the trained CNN is much faster than LS fitting implementation.

Accuracy of the LS algorithm is poor for the CTA dataset, even with the use of cumbersome constrained optimization. Since the CNN estimator can be made robust to deviations from the model assumptions, it shows high, subvoxel accuracy in the case of CTA images as well. In a number of cases, the contours delineated by the observers are apparently placed off the regions of high image intensity. Still, the network can extract such areas in its radius/centerline shift predictions, for further intensity examination, e.g. in search for calcifications.

The obtained results demonstrate the potential usefulness of the CNN as an accurate, fast and robust tool for blood-vessels' lumen quantification – a possible aid to medical diagnosis and automated image annotation. Future studies will focus on the estimator uncertainty analysis, combined with design of training datasets for transfer learning and usage of self-attention architectures to further improve robustness to image imperfections. Collaborative work on applications to other vascularity images, e.g. of the brain, has also been initiated.

References

1. Tsao, C.W. et al.: Heart Disease and Stroke Statistics 2022 Update. Circulation 145, e153e639 (2022). doi: 10.1161/CIR.0000000000001052
2. Lesage, D., Angelini, D.E., Bloch I., Funka-Lea G.: A review of 3D vessel lumen segmentation techniques: models, features and extraction schemes. Medical Image Analysis 13, 819-845 (2009). doi: 10.1016/j.media.2009.07.011
3. Li, H., Tang, Z., Nan, Y., Yang, G.: Human tree-like tubular structure segmentation: A comprehensive review and future perpectives. Computers in Biology and Medicine 151, 106241 (2022). doi: 10.1016/j.compbiomed.2022.106241
4. Schaap, M. et al.: Standardized evaluation methodology and reference database for evaluating coronary artery centerline extraction algorithms. Medical Image Analysis 13(5), 701714 (2009). doi: 10.1016/j.media.2009.06.003
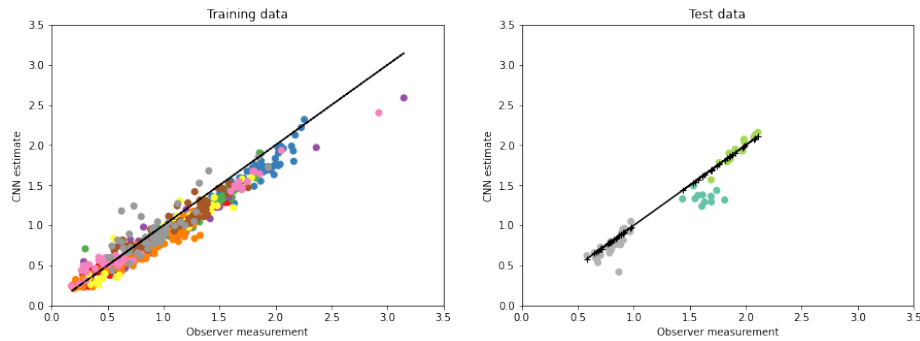
Fig. 5: Scatter plots of training (left) and testing (right) a CNN for estimation of coronary arteries equivalent radius ρ. Horizontal axis: ρ by observer, vertical axis: ρ by the CNN, in mm. Marker color indicates artery segment the input cross-section was sampled from.

5. Cheng, C.P.: Geometric Modeling of Vasculature. Handbook of Vascular Motion, 45-66, Academic Press (2019). doi: 10.1016/B978-0-12-815713-8.00004-8
6. Choi, G., Cheng, C.P., Wilson, N.M., Taylor, C.A.: Methods for Quantifying Three-Dimensional Deformation of Arteries due to Pulsatile and Nonpulsatile Forces: Implications for the Designs of Stenst and Stent Grafts. Annals of Biomedical Engineering 37(1), 14-33 (2009). doi: 10.1007/s10439-008-9590-0
7. Sethian, J.A.: Level Set Methods and Fast Marching Methods. Cambridge University Press (2002)
8. Liu, Y., Kwak, H.S., Oh, I.S.: Cerebrovascular Segmentation Model Based on Spatial Attention-Guided 3D Inception U-Net with Multidirectional MIPs, Applied Sciences, 12, 2288, (2022). doi: 10.3390/app12052288
9. Materka, A. et al.: Automated modeling of tubular blood vessels in 3D MR angiography images. IEEE 9th Int. Symp. On Image and Signal Processing and Analysis, ISPA 2015, pp. 56-61. IEEE, Zagreb (2015). doi: 10.1109/ISPA.2015.7306032
10. Frangi, A.F., Niessen, W.J., Vincken, K.L., Viergever, M.A.: Multiscale Vessel Enhancement Filtering. In Medical Image Computing and Computer-Assisted Intervention MICCAI98, Wells, M. W., Colchester, A., and Delp, S. L. (Eds.), LNCS 1496, pp. 130-137 (1998). doi: 10.1007/BFb0056195
11. Wolterink, J.M., van Hamersvelt, R.W, Viergever, M.A., Leiner, T., Igum, I.: Coronary artery centerline extraction in cardiac CT angiography using a CNN-based orientation classifier. Medical Image Analysis 51, 46-60 (2019). doi: 10.1016/j.media.2018.10.005
12. Chen, Z., Ning, R.: Three-dimensional point spread function measurement of cone-beam computed tomography system by iterative edge-blurring algorithm. Physics in Medicine and Biology 49, 1865-1880 (2004). doi: 10.1088/0031-9155/49/10/003
13. Materka, A., Mizushina, S.: Parametric signal restoration using artificial neural networks. IEEE Transactions on Biomedical Engineering 43(4), 357−372 (1996). doi: 10.1109/10.486256
14. Klepaczko, A., Szczypinski, P., Dwojakowski, G., Strzelecki, M., Materka, A.: Computer simulation of magnetic resonance angiography imaging: model description and validation, PLOS ONE 9(4), e93689 (2014). doi: 10.1371/journal.pone.0093689